cruise, shown in Figure 45. Equating these to the dynamic lift and drag equations yielded Equations 4 and 5.

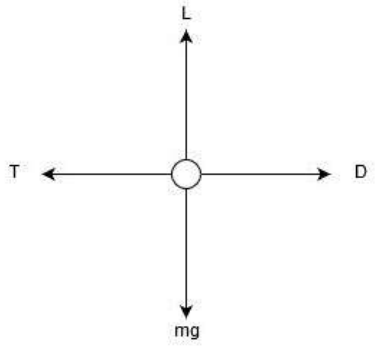

Figure 45: Forces acting on the UAV at cruise

$$L = mg = \frac{1}{2}\rho V^2 S C_L \tag{4}$$

$$T = D = \frac{1}{2}\rho V^2 S C_D = \frac{1}{2}\rho V^2 S C_{D0} + \frac{{C_L}^2}{\pi \cdot AR \cdot e} \tag{5}$$

Calculating the required cruise lift coefficient involved the following assumptions and parameters:

- Civil Aviation Authority (CAA) regulations state that the maximum altitude for a non-commercial UAV is 400ft [15]. At this altitude it is safe to assume that air density if the same as at sea level, hence air density $\rho = 1.225\,\mathrm{kgm}^{-3}$
- Wing area (S), is $0.2\,\mathrm{m}^2$, Aspect Ratio (AR) = 5, efficiency factor (e) = 0.9 and the mass = 1.5 kg
- Stall speed is $6.8\,\mathrm{ms}^{-1}$ and stalls at 13 degrees with a lift coefficient of 1.3
- Cruise speed is $20\,\mathrm{ms}^{-1}$
- From historical data, a suitable value for C_{D0} is 0.032 [16]

Substituting in the above parameters into Equation 4 yielded a lift coefficient of 0.3003. Substituting this lift coefficient into Equation 5 along with the other

parameters yielded a cruise drag value ()D_c) and thus required cruise thrust (T_c) of 1.881 N (91.81 grams of thrust).

The minimum thrust the propulsion system must produce, is set by the design decision that the UAV must be able to climb at the stall speed at an angle of attack of 13 degrees. Therefore, the minimum thrust is given by:

$$T_{\min} = D + mg\sin\alpha \tag{6}$$

Solving this equation using data generated from XFOIL yields the minimum thrust as 4.26 N. After applying a safety factor of 20 %, the minimum thrust rises to 5.11 N. This equates to 521 grams of thrust. The CFD analysis validated these assumptions and results meaning the thrust calculations will be accurate for the physical model and hence were used to design the propulsion system.

4.2 Motor Comparisons

The two main propulsion systems for remote controlled aircraft are electric motors and nitro or gas engines. Nitro or gas-powered engines are inherently heavy due to being combustion engines and require a fuel tank, however, for larger models this is offset by the huge thrust they output in comparison with an electric motor. For small models however, nitro/gas engines are difficult to implement due to their weight, their need for a large take off area and their low efficiency in comparison with electric motors. Therefore, electric motors have been chosen for this project.

Electric motors themselves can then be split into two sections, brushless or brushed motors. The key differences between the two are:

- For brushless motors, the rotor spins around the inner stator coils whereas for brushed motors, the rotor spins within the outer stator magnets increased speed over brushless motors.
- Brushless motor efficiency is between 85-90 %.

- Brushed motor efficiency is between 75-85 %.
- Reduced brushed efficiency due to the friction between the brushes and the commutator, causing the brushes to eventually wear out.
- The switching of contact between commutator and the brushes causes increased electromagnetic (EM) noise – bad for EM sensitive components such as the GPS.
- Brushless motors can produce more torque and thus spin larger propellers due to the increased motor diameter.
- Brushless motors require Electronic Speed Controllers (ESCs) and are therefore more expensive than brushed motors.

Combining these analyses with market research shows that most brushed motors are for ground vehicle operations and so none were suitable for this project. Therefore, this UAV will be powered using two brushless electric motors, each producing half the required thrust and will act as pull motors. There were only two motors that fulfil the UAV thrust requirements and that come with valid thrust tests. Therefore, a comparison has been made between the EMAX MT2213 and MT2216 motors shown in Figure 46.

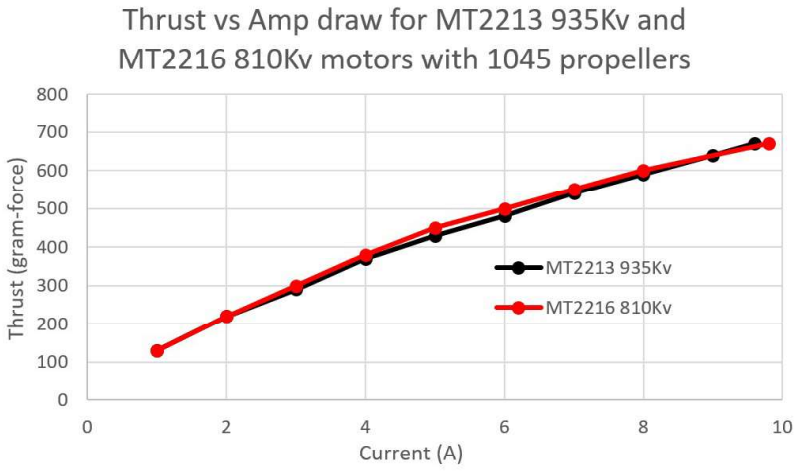

Figure 46: Thrust vs current of 935Kv and 810Kv motors when using 1045 propellers

The provided thrust data showed that whilst spinning a 1045 propeller (10-inch diameter propeller with a 4.5-inch pitch) both motors performed almost

identically with the 810 Kv motor having an increase in thrust of only 10 g at currents between 4 and 8 A. The efficiency of each motor was then calculated from the thrust data and plotted in Figure 47 to show how the efficiency changed when the current drawn by the motor varies.

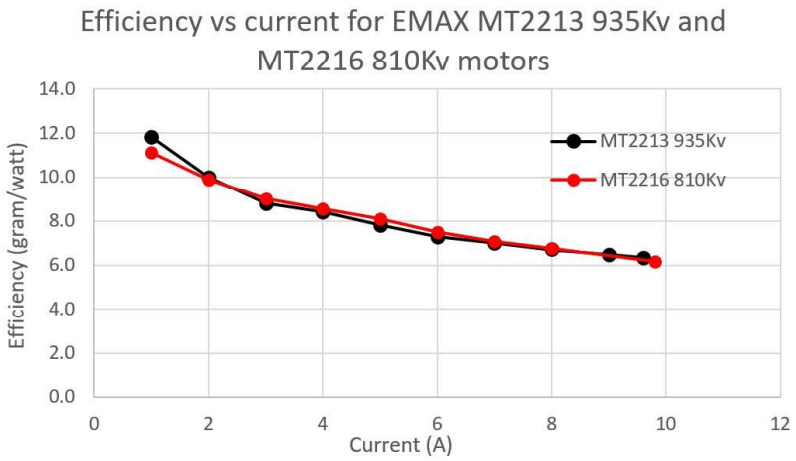

Figure 47: Efficiency of 935Kv and 810Kv motors vs current drawn when using 1045 propellers

Figure 47 shows that the 935 Kv motor is 6.4 % more efficient at 1 A and slightly more efficient up to a current of 2 A. The 810 Kv motor on the other hand, is slightly more efficient at all other current values. However, since the UAV will spend most of the mission at cruise, each motor will only be required to draw 1 A to yield the cruise thrust of 191.81 g of thrust, so low current draw efficient values are more important than the efficiencies at higher currents.

The 935Kv motor is 11.3 % lighter (7 g) than the 810 Kv motors, meaning the total weight saving is 14 grams. Whilst this is a small decrease, it will help to make the UAV more stable in the roll axis due to the reduced moment required to roll.

Another advantage of the 935 Kv motors over the 810 Kv motors is that they come in clockwise or counter-clockwise variants. This means that each individual motor can rotate oppositely to each other, thus eliminating the rolling effect caused by engine torque that occurs when using a single motor setup. The reason they can do this is because the motor thread and mounting-nut thread can be in the same direction, so the rotation of the motor effectively causes the nut to tighten, thus eliminating the possibility of a propeller coming loose during

flight.

Due to these reasons, two 935 Kv motors will be chosen for the propulsion system.

4.3 Propellers

Every brushless electric motor comes with a Kv value. This value corresponds to the number of revolutions per minute (rpm) the un-loaded motor turns when a voltage of 1 V is applied across it. The 935 Kv motors chosen for the propulsion system have a relatively low Kv value and so they would not be able to spin small propellers at a high enough rotational velocity to provide the required lift. To understand what type of propeller would provide better performance for this propulsion system, the thrust data when using an 8045 and 1045 propeller was analysed and shown in Figure 48 [17], [18].

The first two digits give the diameter of the propeller in inches and the final two digits give the pitch of the propeller, where the pitch corresponds to the distance in inches traversed in air, after the propeller has performed one full rotation. To reduce the current drawn by the motors whilst retaining the same propeller diameter, the pitch must be reduced, however, reducing the pitch reduces the maximum thrust of the motor. Reducing the diameter of the propeller whilst maintaining the pitch has the same effect, this can be seen in 48 and Figure 49. They show the thrust and efficiency of the 935 Kv motors when using 1045 and 8045 propellers. It is clear to see that these motors perform best when using a larger diameter of propeller due to their relatively slow rotational speed.

48 also shows that the maximum thrust using an 8045 propeller is significantly lower at 490 g as the maximum rotational velocity has been achieved. This does yield a lower current for maximum thrust, however this is irrelevant as it is 180 g less thrust than when using the 1045 propeller.

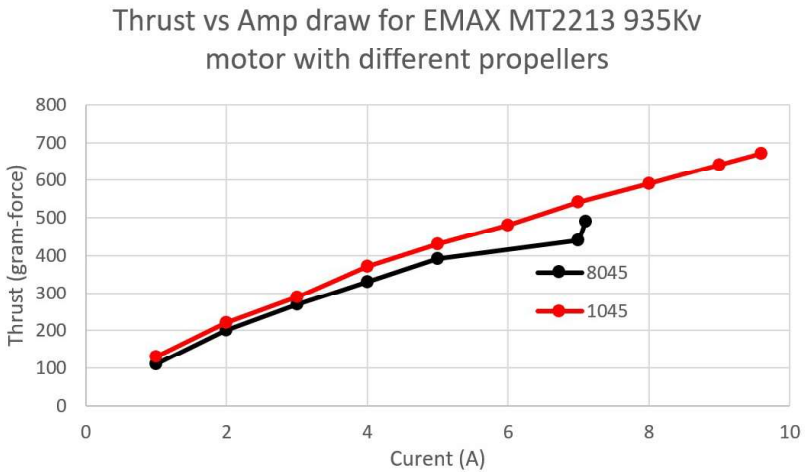

Figure 48: Thrust vs current for 935Kv motors when using 8045 and 1045 propellers

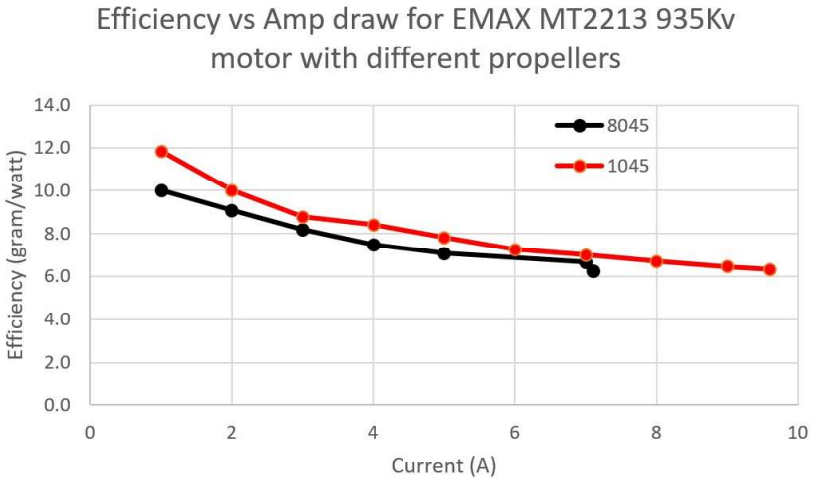

Figure 49: Efficiency of 935Kv and 810Kv motors vs current when using 8045 and 1045 propellers

4.4 Electronic Speed Controllers (ESCs)

The ESCs are required to translate a signal from the flight controller to a switching frequency that will cause the desired speed of the motor to be achieved. The 935 Kv motors chosen are brushless meaning they each require a brushless speed controller. The ESCs need to each be able to sustain the maximum current that the motors can each draw from the battery. At maximum throttle using a 1045 propeller, the maximum current draw is 9.6 A so each ESC must be rated to at least this number. The chosen ESCs for this UAV are KISS 25-amp ESCs

due to being incredibly light at only 3 g each and being able to provide over twice the current each motor could possibly draw. The KISS brand is well established and KISS products come with ample documentation so should ease troubleshooting any issues during the manufacturing of the UAV.

4.5 Battery Selection

For remote controlled aircraft of this type, by far the most commonly used battery technology is Lithium Polymer (Li-Po). These provide good energy densities and different power outputs at many different voltages. Li-Po batteries are specified in terms of their nominal voltage which is dictated by their cell count. Each cell has a minimum voltage of 3.9 V and once fully charged, the voltage of each cell is 4.2 volts. Therefore, a 3 cell Li-Po battery will have a nominal voltage of 11.1V and a maximum voltage of 12.6 V. The thrust data for the EMAX MT2213 935 Kv motors is provided for when the supplied voltage is nominal for a 3 cell Li-Po battery – 11.1 V. This means that the maximum output of the motors will be increased due to the increased voltage of a fully charged battery, however, this increase will not be large enough to increase the current drawn to levels exceeding the ESCs maximum current capability.

Each Li-Po battery is defined by the following Li-Po features:

- Cell count
- Nominal voltage
- Milli-Ampere hour capacity (mAh)
- C rating (C)

The mAh rating defines the amount of current that the battery can provide for one hour and is a measure of the energy held within the battery. The C rating is used in conjunction with the mAh capacity to define the maximum continuous current the battery can output. This is done by multiplying the C rating by the

Ah rating. For example, a battery with a capacity of 5000 mAh (5 Ah) and a C rating of 10 results in a maximum continuous output current of 50 A.

For this UAV, the propulsion system requires the greatest power and current of all the electronics, so the battery must be able to provide at least this current, which is approximately 20 A.

From the approved manufacturers list, the available batteries were tabulated in terms of the most important factors and rejected from contention if they were heavier than 200 g or if the battery dimensions were too large for the internals of the fuselage. This is shown below in Figure 50.

Brand	Nominal volatage (V)	mAh	C rating	Max continuous current (A)	Flight time (mins)	Mass (g)	Flight time > 10 mins?	Mass greater than 200g?	Dimensions too large for fuselage?
Gens-Ace	11.1	800	40	32	6.11	72	N	N	N
Gens-Ace	11.1	1000	25	25	7.64	96	N	N	N
Gens-Ace	11.1	2200	25	55	16.80	183.7	Y	N	N
Gens-Ace	11.1	3000	25	75	22.91	297.2	Y	Y	N
Gens-Ace	11.1	5200	10	52	39.71	315	Y	Y	Y
Tattu	11.1	1050	75	78.75	8.02	130	N	N	N
Tattu	11.1	1300	45	58.5	9.93	120	N	N	N
Tattu	11.1	1550	45	69.75	11.84	135	Y	N	N
Tattu	11.1	5100	10	51	38.95	331	Y	Y	Y

Figure 50: Battery decision table

The flight time was calculated using the mAh rating and a series of assumptions about the dynamics of the mission. The assumptions being:

- Current is purely drawn from the motors as other components will draw a relatively small amount of current
- Battery is fully charged at the beginning of the mission and is discharged to 70 % of its maximum capacity – this will allow for landing with reserve power as well as protect the battery from over discharging
- The UAV will operate at maximum thrust (20 A) 10 % of the time, 50 % thrust (10 A) 10 % of the time, 25 % thrust for 30 % of the time and at cruise thrust for 50 % of the time. This yielded a mean current draw of 5.5 A

From the Battery decision table, it is clear to see that two batteries fulfilled all the criteria for this UAV project. The Gens-Ace 2200 mAh 25C and Tattu 1550 mAh 45C batteries. The Tattu battery has maximum current value 14.75 A

larger than the Gens-Ace battery and is 48.7 g lighter. However, the Gens-Ace battery can provide a flight time 42 % greater than that of the Tattu battery. This is more important than the Tattu advantages, as both can still provide the maximum required current of 20 A and the 5-minute increase of flight time far outweighs the 48.7 g mass deficit.

Therefore, one 3-cell Gens-Ace 2200 mAh battery pack will be used for this UAV.

4.6 Power Distribution

The ESCs and the motors will be supplied straight from the Li-Po battery meaning they will operate at the battery voltage of 12 V. They will be connected to the battery via a power module, that will measure the voltage and current drawn during operation and send the data back to the Navio2 flight controller for telemetry purposes. The power module has a built in UBEC (Universal Battery Eliminator Circuit) to step the battery voltage of 12 V down to 5 V which will be used to power the 5 V electronics. The UBEC will be directly connected to the Navio2 board so it can distribute the 5 V to all the servos, the 2.4 GHz radio receiver, the 433 MHz telemetry transmitter, the airspeed sensor and the GPS antenna. The 5.8 GHz video transmitter can be powered using a 5-18 V voltage range and will also provide a clean 5 V output to the MinimOSD and the FPV camera, therefore it will be directly connected to the battery.

For clarity, the power distribution layout has been summarised by Figure 51. Note that this is how power is distributed alone and not how the electronic devices interact with each other.

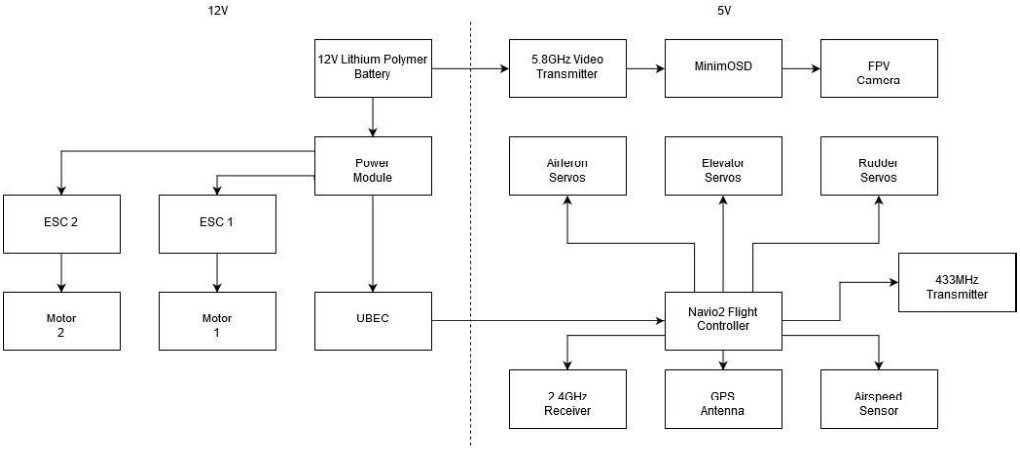

Figure 51: Power distribution layout of the UAV

5 Electronics, Control and Communication

5.1 Communication between the UAV and groundstation

The UAV will be controlled by the user via a 2.4 GHz Futaba T6K radio transmitter and will be received by a 7-channel R617FS receiver onboard the UAV. The first four channels will be used to manually control the throttle, roll, pitch and yaw positions. The other 3 channels will be used as auxiliary inputs to switch between autonomous modes within in the flight controller. The inputs from the user will then be sent to the flight controller to perform the users request by sending PWM signals to the servos and speed controllers.

During either autonomous or manual flight, the live status of the UAV will be measured by onboard sensors and streamed to the groundstation where it will be viewed by the user on a computer and a live video feed. The computer receives telemetry data from the drone via a 433 MHz telemetry link and the telemetry will be viewed using Mission Planner software. The live video feed will be transmitted at a frequency of 5.8 GHz from the UAV but will have telemetry data superimposed on the image from the camera.

Figure 52 illustrates how each communication mechanism will interact between the UAV and the groundstation.

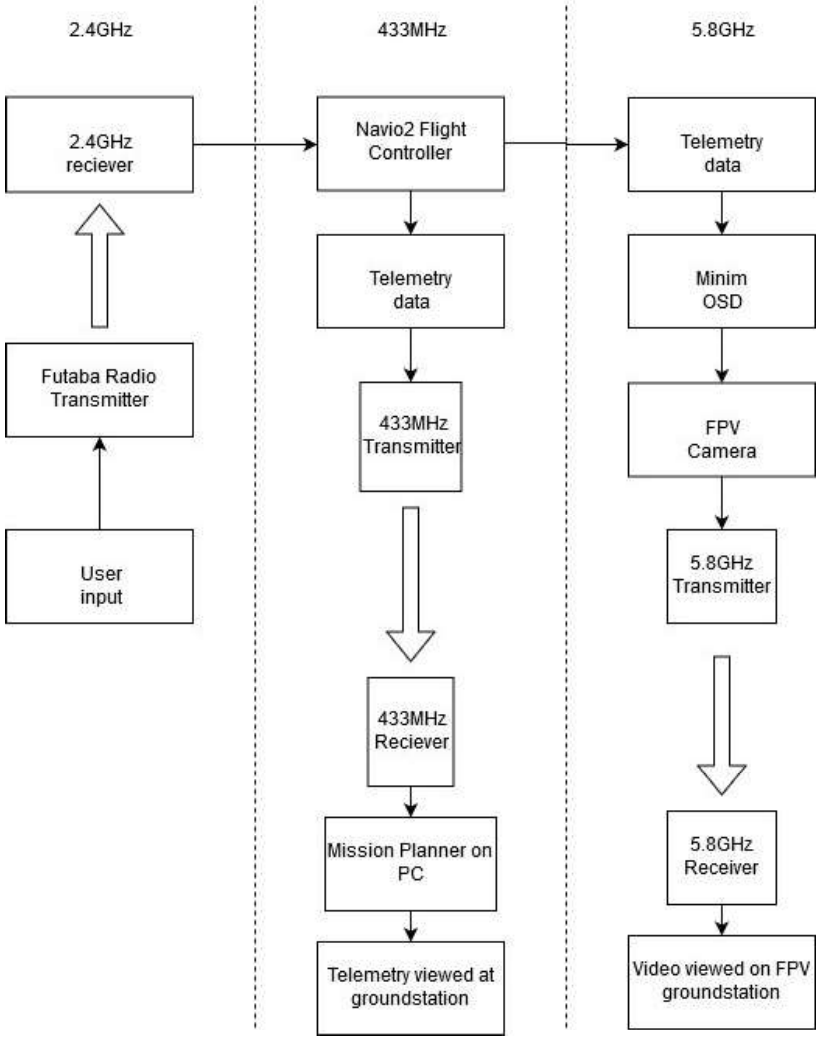

Figure 52: UAV Communication layout

Each of the three communication mechanisms used to communicate with the UAV will operate within a set frequency band, where the frequency band and corresponding maximum radiated output power is set and restricted by Ofcom [19]. The restrictions on each frequency are shown below:

The 2.4 GHz Futaba radio transmitter operates at 100 mW as standard which can provide a range of up to 4 km. Like with all radio communication however, this is heavily dependent upon external conditions such as EM noise and objects intercepting the radio signals. The 100 mW limit on the 433 MHz telemetry system limits the option choices from the approved manufacturers list to a system that will only provide a maximum range of 1 km. The 5.8 GHz link is lim-

Frequency (MHz)	Frequency band (MHz)	Maximum frequency bandwidth (KHz)	Maximum radiated output power (mW)
433	433.050 - 434.79	25	100
2400	2400 - 2483.5	N/A	100
5800	5725 - 5875	N/A	25

Figure 53: Summary of restrictions upon frequencies used for communications with the UAV

ited to a small 25 mW resulting in a range of around 1 km. The quality of the video feed is quite low when using linearly-polarised omni-directional antennas since the receiver and transmitter antennas must be aligned to maximise the radiation overlap, however this is not often achieved during flight. Therefore, using circularly-polarised omni-directional antennas rather than linearly-polarised antennas means that overlap is always achieved regardless of the UAV orientation, resulting in a higher quality of video feed. The circularly-polarised signal transmitted can either be Left Hand Circularly Polarised (LHCP) or Right Hand Circularly Polarised (RHCP). The left or right corresponds to the rotation of the corkscrew signal and must be matched between the transmitter and receiver antennas.

The range of the video feed can be increased by using a directional patch antenna. The downside of using one of these is that to receive the signal, the antenna must be pointing at the transmitter. This alone would not be suitable for the receiver at the groundstation as it is not feasible to constantly adjust the antenna to point at the aircraft. Therefore, a combination of both an omni-directional and directional antenna would give the best overall coverage. To achieve this, a diversity receiver must be used to switch between the antennas and display the signal on screen from the antenna that is receiving the best quality signal from the transmitter.

Figure 54 shows the groundstation setup used to obtain a high-quality video feed.

The gain of the circularly polarised antenna is a measure of its power and this must be considered when choosing antennas for the video groundstation. By increasing the gain of an antenna (measured in decibels), this effectively

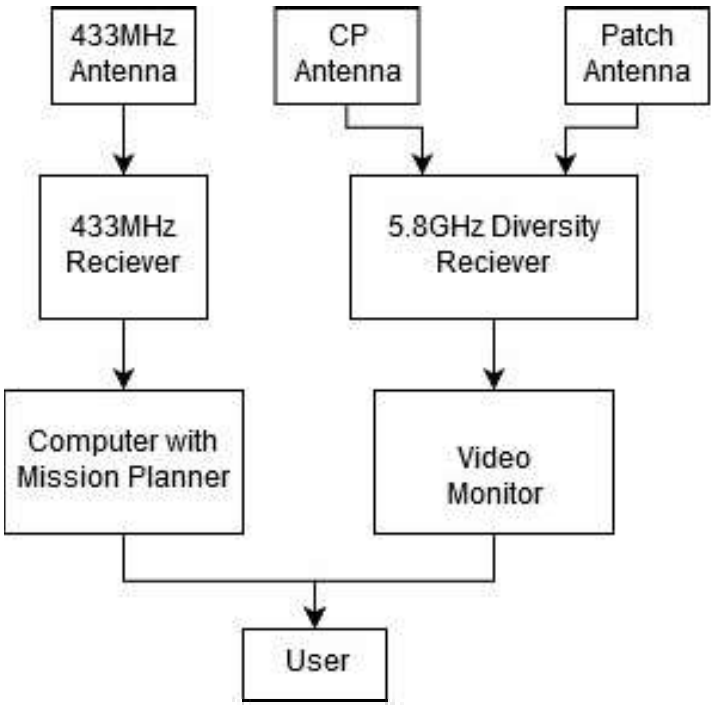

Figure 54: Groundstation setup

stretches out the radiation pattern into a form that increases range but reduces coverage. This is best shown using the Figure 55 and Figure 56 below [20]:

The vertical graph in Figure 55 shows what the coverage looks like when looking at the omni-directional antenna pointing up. It shows good coverage for everywhere aside from when the antenna is roughly pointing at the incoming signal. The horizontal graph shows the coverage when looking directly down the antenna and shows the horizontal coverage is ideal.

The range of the antenna is increased when the gain is increased. This is because a large gain narrows the radiation pattern of the antenna. As the radiation pattern narrows, the antenna becomes directional and hence the vertical and horizontal coverage of the antenna looks like Figure 56 below:

This UAV is not required to have extreme video range and therefore, the gain of the patch antenna can be low to still retain a wide radiation pattern. Therefore, the patch antenna chosen is a 5 dB TBS antenna as the supplied data-sheet states a real-world range of 1.5km, whilst retaining a wide radiation pattern of 110 degrees. This is feasible for the UAV to remain in during flight. The transmitter

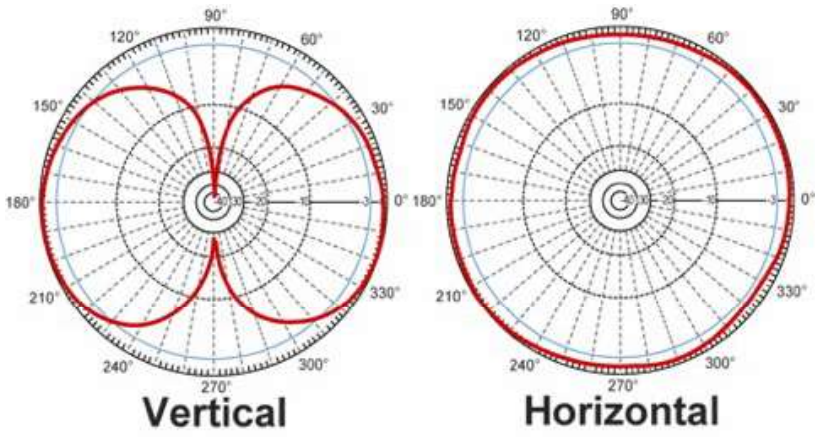

Figure 55: Omni-directional antenna (with a gain of 3dB) vertical and horizontal radiation pattern

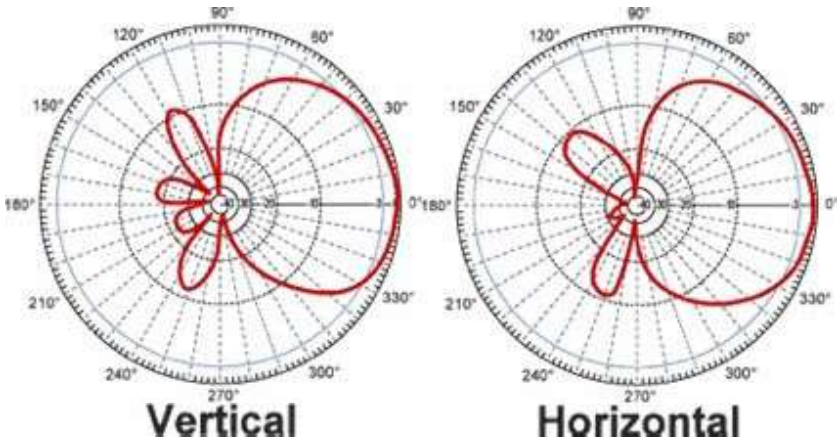

Figure 56: Directional antenna vertical and horizontal radiation pattern coverage

and receiver omni-directional antennas chosen are TBS 1.26 dB antennas meaning these will provide great coverage when the UAV is within approximately 1km of range. All the video antennas stated are RHCP antennas meaning they will all be compatible with one-another.

The video receiver must be connected to a monitor that can remain on, even when the signal degrades to a very low level. Most monitors have a function where the display will switch to a blue screen if the input source becomes weak. This is dangerous for the UAV as the video feed will inevitably have periods of poor signal quality, meaning a normal screen would not continue to display the video feed which could cause loss of control. Therefore, a non-bluescreen monitor must be used. Monitors that have this feature are either incorporated

into First Person View (FPV) goggles which are very expensive. Therefore, the choice of monitor is a 7-inch monitor with a built-in battery and diversity receiver. This will simplify the groundstation and make transporting the equipment to and from the testing areas much easier.

5.2 Actuators

Due to the small mass of the aircraft, the forces upon the control surfaces are relatively small, meaning light servos can be used for actuation. The number of servos that are suitable for this UAV are very large and hence a decision was made to have high-quality digital servos from a reputable brand. EMAX 12 g metal gear instead of plastically geared servos were therefore chosen as they are more resistant to wear over time, meaning that the actuation is more reliable and a loss of control due to gear wear is less likely.

Each aileron and rudder will be actuated by a single servo as each servo provides enough torque to move the entire control surface. The elevator is significantly larger than the aileron and rudder control surfaces and so will be actuated by two servos. This only adds approximately 12 g to the weight of the UAV and so is justified to help prevent elevator servo wear.

5.3 Autopilot and Autonomy Sensors

The level of autonomy was decided to be high and so a powerful flight controller with the ability to add external sensors was required. The Ardupilot APM2.8 flight controller has very good documentation, however is made using only an 8-bit processor and is no longer supported by Ardupilot. The other option was to choose a Raspberry Pi based board and so the Navio2 by Emlid was chosen. The Navio2 is a shield that is mounted directly onto the Raspberry Pi and uses the well-supported and stable Ardupilot software. The Navio2 is much more powerful than the APM board since a Raspberry Pi uses a quad-core processor in a Linux based environment, meaning a much greater level of control and autonomy can be achieved. The Navio2 comes with all the required sensors for

stabilised manual flight but also inbuilt sensors for autonomy, these include a barometer and a GPS module. To achieve the desired level of autonomy, an airspeed sensor is required to obtain an accurate measurement of the UAV true air-speed, otherwise the speed would be the equivalent air-speed (ground speed) which is calculated using GPS data and this could cause inaccuracies when flying in autonomous mode.

The Navio2 will be controlled using the latest firmware from the Ardupilot Mission Planner software. This will allow the user to see real time the UAV heading, altitude, attitude, GPS location, GPS signal quality and ground speed. Mission Planner allows live control of the UAV by changing or adding waypoints whilst in the air and enables the user to take manual control for when the pilot wants to bring the UAV into land.

5.4 Avionics layout

The decision upon the location of each electrical component is governed by their most impactful characteristics. For example, an ESC produces a lot of electromagnetic (EM) noise however weighs only a few grams, therefore its position is not based on centre of gravity but on minimising interference with other components.

The motors and the ESCs are the greatest producer of EM noise due to the large current flowing through them, so each motor and ESC pair has been placed as far away as possible from the central fuselage, to minimise the interference they may cause with the three communication systems and the flight controller. Each communication system operates within a different frequency band however interference will still occur between each signal, therefore each transmitter or receiver has been placed away from one-another to minimise this interference.

Due to the lightweight nature of the camera and OSD, they can be placed near the front of the fuselage meaning the camera is in the correct position to capture the best point-of-view (POV) for the user to fly from. The camera itself comes on a small bracket that allows the pitch angle of the camera to be adjusted

meaning the user can tailor the angle to suit their preference. The lightweight air-speed sensor will also be placed towards the front of the fuselage, so that the incoming air pressure is more accurately measured since there will be less interference from the rest of the UAV structure. This will give a more accurate true-airspeed of the UAV and will result in more accurate autonomy.

The Navio2 and Raspberry Pi will be placed at the centre of mass to make sure that the accelerometers correctly read what is happening to the attitude of the UAV as this will give more accurate autonomy. They will also be placed within the fuselage to make sure the sensitive components are well protected against external weather conditions. Most of the electrical components are very light, however the Li-Po battery is an exception. At over 10 % of the total UAV mass, the battery will be placed as close to the aerodynamic centre as possible minimising the distance between the aerodynamic centre and centre of mass. The servos are not waterproof therefore each will be placed within the airframe to be as well protected against external conditions as possible. To achieve this, extra-long control horns will be used whilst retaining the same torque.

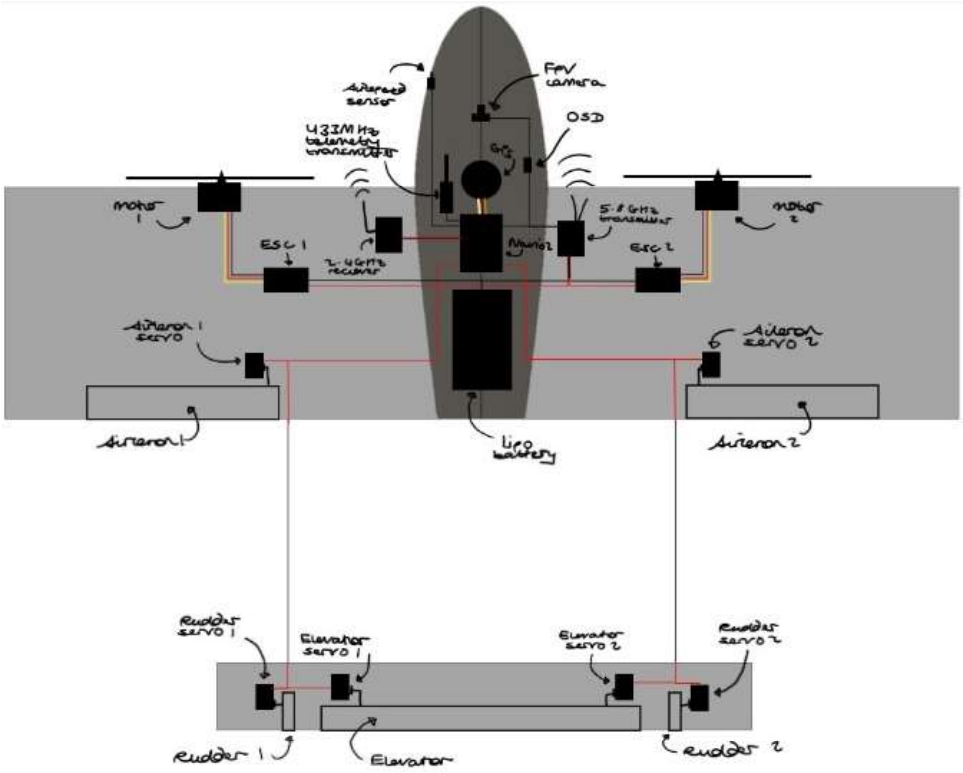

Figure 57: Layout of the UAV electrical components

6 Conclusion

Following completion of the design, a bill of materials was produced (below). This contains all the parts needed to produce the aircraft and where they will be purchased from. This gives an estimated cost of the entire aircraft of 755 and a total estimated mass of 1026 g. This falls comfortably between both criteria.

Section	Item	Quantity	Item price (£)	Total Price (£)	Indiviual mass (g)	Total mass (g)	Supplier
Control	Navio2 flight controller	1	£149.99	£149.99	23	23	Unmanned Tech
	Navio2 Wire Pack	1	£8.00	£8.00	5	5	Unmanned Tech
	Navio2 GPS Antenna	1	£17.00	£17.00	5	5	Unmanned Tech
	Navio2 Power Module	1	£14.99	£14.99	22	22	Unmanned Tech
	Raspberry Pi 3 Model B+	1	£34.00	£34.00	50	50	Cool Components
	433MHz Telemetry kit (100mW)	1	£27.99	£27.99	5	5	Unmanned Tech
	Airspeed sensor	1	£20.99	£20.99	20	20	Unmanned Tech
	Minim OSD Micro	1	£7.50	£7.50	5	5	Unmanned Tech
	Header-Pins	1	£1.75	£1.75	5	5	Unmanned Tech
Propulsion and control surafaces	935Kv motor (one CW and one CCW)	2	£9.95	£19.90	55	110	Unmanned Tech
	KISS 25A ESC	2	£20.93	£41.86	2	4	Unmanned Tech
	Gens-Ace 2200mAh battery	1	£17.99	£17.99	183.7	183.7	Unmanned Tech
	EMAX ES08A II Servos	6	£7.99	£47.94	12	72	Unmanned Tech
	1045 Propellers (Carbon-fibre reinforced)	2	£3.49	£6.98	5	10	Unmanned Tech
	1046 Propellers (Plastic)	2	£1.00	£2.00	5	10	Unmanned Tech
FPV Video Setup	FPV Camera	1	£25.85	£25.85	14	14	Unmanned Tech
	FPV Transmitter (SMA FEMALE)	1	£34.70	£34.70	5	5	Unmanned Tech
	FPV Antenna pair (SMA MALE RHCP)	1	£24.90	£24.90	11.5	11.5	Unmanned Tech
	FPV Patch Antenna (SMA MALE RHCP)	1	£11.90	£11.90	N/A	N/A	Unmanned Tech
	FPV Monitor/Receiver	1	£109.99	£109.99	N/A	N/A	Unmanned Tech
Useful extras	Raspberry Pi Power Supply	1	£8.34	£8.34	N/A	N/A	Cool Components
	SD Card (For Raspberry Pi)	1	£10.00	£10.00	2	2	Cool Components
	Heat shrink tubing	1	£3.99	£3.99	2	2	Unmanned Tech
	SMA extenders/adapters	1	£1.75	£1.75	N/A	N/A	Unmanned Tech
Main Structure	Carbon spars - wing front	1	£9.20	£9.20	27	27	Easy Composites
	Carbon spars - wing rear	1	£8.60	£8.60	35	35	Easy Composites
	Carbon spars - tail	1	£3.30	£3.30	11	11	Easy Composites
	SolarSpan	2	£10.99	£21.98	40	40	ServoShop
	Birch Plywood 6mm x 300x900mm	2	£5.25	£10.50	N/A	30	Balsa Cabin
	Birch Plywood 3mm x 300x900mm	2	£3.60	£7.20	N/A	30	Balsa Cabin
	Foam	3	£13.75	£41.25	40	120	ServoShop
3D Printed:	Motor mount	2	£0.50	£1.00	25	50	RS Components
	Aileron	2	£0.60	£1.20	30	60	RS Components
	Aileron skin break	2	£0.16	£0.32	8	16	RS Components
	Tail spar mount	6	£0.01	£0.04	0.3	1.8	RS Components
	Tail ends	2	£0.16	£0.32	8	16	RS Components
	Wing centre/dihedral	1	£0.50	£0.50	25	25	RS Components

TOTAL IN FLIGHT MASS	**1026g**
TOTAL PRICE (Excluding Delivery costs)	**£755.71**

Addittionally, a Gantt chart was produced for the planned construction process 58. This will help ensure that the project will be completed in time and help the manufacturing process go smoothly.

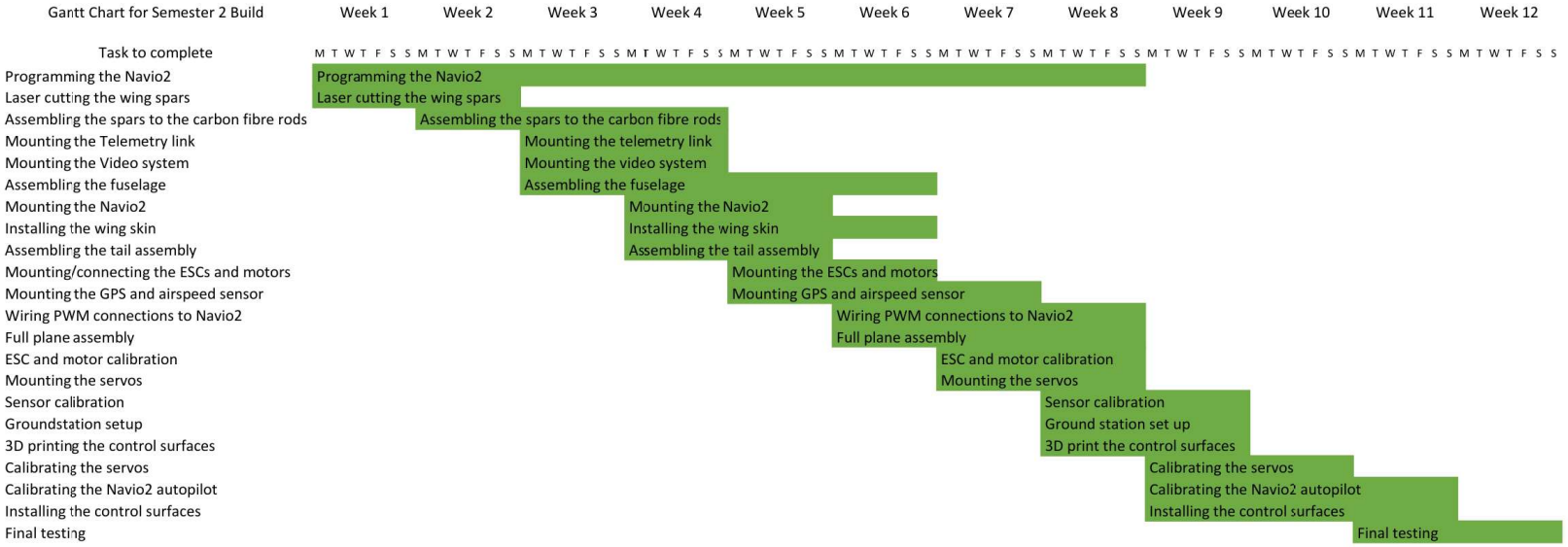

Figure 58: Gantt chart of planned construction process

Throughout the design of this UAV, all aspects of a modern autonomous aerial vehicle were considered and detailed within this report.

- A CAD prototype was decided upon and analysed for its structure and aerodynamics, where improvements would be made to achieve greater efficiency and structural strength.
- A Finite Element Analysis (FEA) was performed on the main structures of the CAD model to prevent structural failure during flight.
- Based upon the FEA analysis, materials were chosen for the aircraft that support the strength of the structure, whilst maintaining a low mass for the aircraft.
- The main wing, tail, fuselage and full CAD model were then analysed in CFD, to find any areas where the design caused high drag and suggest were improvements could be made to the aerodynamic design of the UAV.
- Any improvements made were a compromise between structural strength and aerodynamic efficiency.
- The required propulsion and power distribution system were then designed to propel the UAV, based upon assumptions of how the aircraft would be flown.
- The level of autonomy decided upon was high and so a powerful flight-controller with a GPS and airspeed-sensor are included.
- Communication with the UAV was designed to increase range and redundancy for important telemetry data, as the telemetry is vital for correct operation during autonomous missions.
- The electrical components were chosen based upon the most important factors for the UAV; weight, communication interference, range and efficiency.
- All the electrical components chosen are CAA legal, meaning the UAV can be certified and legally flown as per CAA regulations.

This final design for the UAV will be taken to the manufacturing stage next semester, however alterations may occur due to issues that may arise during manufacturing.

References

[1] *Carbon Fibre Square Box Section*, [Online; accessed 01. Dec. 2019], Dec. 2019. [Online]. Available: https://www.easycomposites.co.uk/#!/cured-carbon-fibre-products/carbon-fibre-box-section/carbon-fibre-box-section-8mm-7mm.html.

[2] *CES EduPack | Granta Design*, [Online; accessed 02. Dec. 2019], Dec. 2019. [Online]. Available: https://grantadesign.com/education/ces-edupack.

[3] M. F. Ashby, K. E. Easterling, R. Harrysson, and S. K. Maiti, "The Fracture and Toughness of Woods," *Proceedings of the Royal Society of London. Series A, Mathematical and Physical Sciences*, vol. 398, no. 1815, pp. 261–280, Apr. 1985, ISSN: 0080-4630. DOI: 10.2307/2397514.

[4] *ANSYS sample materials data | Granta Design*, [Online; accessed 01. Dec. 2019], Dec. 2019. [Online]. Available: https://grantadesign.com/industry/products/granta-mi/product-engineering/granta-misimulation/material-intelligence-in-ansys-workbench/sample-materials-data-for-ansys-workbench.

[5] *Solarspan*, [Online; accessed 28. Nov. 2019], Dec. 2019. [Online]. Available: https://solarfilm.co.uk/products/solarspan.

[6] V. E. Kuznetsov, A. N. Solonin, O. D. Urzhumtsev, R. Schilling, and A. G. Tavitov, "Strength of PLA Components Fabricated with Fused Deposition Technology Using a Desktop 3D Printer as a Function of Geometrical Parameters of the Process," *Polymers*, vol. 10, no. 3, p. 313, Mar. 2018, ISSN: 2073-4360. DOI: 10.3390/polym10030313.

[7] M. Harris, J. Potgieter, R. Archer, and K. M. Arif, "Effect of Material and Process Specific Factors on the Strength of Printed Parts in Fused Filament Fabrication: A Review of Recent Developments," *Materials*, vol. 12, no. 10, May 2019. DOI: 10.3390/ma12101664.

[8] S. J. Loring, "General Approach to the FLUTTER PROBLEM," *SAE Trans.*, vol. 36/49, pp. 345–356, 1941, ISSN: 0096-736X. DOI: 10.2307/44438865.

[9] X. Qi, Q.-S. Peng, C.-S. Zhao, and F.-F. Zhang, "A new method based on attitude quaternion matching for transfer alignment," *ResearchGate*, vol. 32, no. 1, pp. 81–87, Jan. 2011. DOI: 10.3873/j.issn.1000-1328.2011.01.012.

[10] K. Cheng, *Machining Dynamics - Fundamentals, Applications and Practices | Kai Cheng | Springer*. Springer-Verlag London, 2009, ISBN: 978-1-84628-367-3. DOI: 10.1007/978-1-84628-368-0.

[11] *xfoil Python module*, [Online; accessed 23. Nov. 2019], Nov. 2019. [Online]. Available: https://pypi.org/project/xfoil.

[12] *ANSYS FLUENT 12.0 Theory Guide - 4.11.2 Filtered Navier-Stokes Equations*, [Online; accessed 03. Dec. 2019], Feb. 2010. [Online]. Available: https://www.afs.enea.it/project/neptunius/docs/fluent/html/th/node94.htm.

[13] *ANSYS FLUENT 12.0 User's Guide - 7.3.15 Symmetry Boundary Conditions*, [Online; accessed 03. Dec. 2019], Feb. 2010. [Online]. Available: https://www.afs.enea.it/project/neptunius/docs/fluent/html/ug/node251.htm.

[14] *ANSYS FLUENT 12.0 User's Guide - 7.3.14 Wall Boundary Conditions*, [Online; accessed 03. Dec. 2019], Feb. 2010. [Online]. Available: https://www.afs.enea.it/project/neptunius/docs/fluent/html/ug/node250.htm.

[15] *CAP 658: Model Aircraft: A Guide to Safe Flying*, [Online; accessed 05. Dec. 2019], Dec. 2019. [Online]. Available: https://publicapps.caa.co.uk/modalapplication.aspx?appid=11&mode=detail&id=5631.

[16] D. P. Coiro and F. Nicolosi, "Design of a Three Surfaces R/C Aircraft Model," *Acta Polytechnica*, vol. 42, no. 1, Jan. 2002, ISSN: 1805-2363. DOI: 10.14311/314.

[17] *Brushless Motor Emax MT2213 935Kv*, [Online; accessed 05. Dec. 2019], Nov. 2014. [Online]. Available: https://www.unmannedtechshop.co.uk/product/brushless-motor-emax-mt2213-935kv.

[18] *MT2216 810Kv Muticopter Motor*, [Online; accessed 05. Dec. 2019], Nov. 2014. [Online]. Available: https://www.unmannedtechshop.co.uk/product/mt2216-810kv-muticopter-motor.

[19] *Radio-controlled models*, [Online; accessed 04. Dec. 2019], Feb. 2018. [Online]. Available: https://www.ofcom.org.uk/spectrum/radio-spectrum-and-the-law/licence-exempt-radio-use/licence-exempt-devices/Radio-controlled-models.

[20] *The complete guide to FPV antennas for your drone*, [Online; accessed 04. Dec. 2019], Dec. 2015. [Online]. Available: https://www.dronetrest.com/t/the-complete-guide-to-fpv-antennas-for-your-drone/1473.